Lagrangian Statistics for Dispersion in Magnetohydrodynamic Turbulence

J. Pratt[1], A. Busse[2], W.-C. Müller[3]

[1]Georgia State University, Department of Physics and Astronomy, Atlanta Georgia, 30303, USA
[2]James Watt School of Engineering, University of Glasgow, Glasgow G12 8QQ, United Kingdom
[3]Center for Astronomy and Astrophysics, ER 3-2, TU Berlin, Hardenbergstr. 36, 10623 Berlin, Germany

Key Points:

- We perform direct numerical simulations of isotropic and anisotropic magnetohydrodynamic turbulence.
- We examine and compare single-particle diffusion, two-particle dispersion, and many particle dispersion.
- Our Lagrangian statistics reveal the dependence of anisotropy on separation time scales from the Lagrangian point of view.

Corresponding author: J. Pratt, jpratt7@gsu.edu

Abstract
Measurements in the heliosphere and high-resolution fluid simulations give clear indications for the anisotropy of plasma turbulence in the presence of magnetic fields. How this anisotropy affects transport processes like diffusion and dispersion remains an open question. The first efforts to characterize Lagrangian single-particle diffusion and two-particle dispersion in incompressible magnetohydrodynamic (MHD) turbulence were performed a decade ago. We revisit those pioneering results through updated simulations performed at higher Reynolds number. We present new investigations that use the dispersion of many Lagrangian tracer particles to examine the extremes of dispersion and the anisotropy in direct numerical simulations. We then point out directions in which Lagrangian statistics need to be developed to address the fundamental problem of anisotropic MHD turbulence and transport in solar and stellar winds.

1 Introduction

To understand solar or stellar winds, we first study the fundamental behavior of a turbulent plasma. Understanding the anisotropic dynamics of a turbulent plasma is key to producing predictions and models for the scattering of energetic particles in a solar wind. In his famous book on turbulence (Lesieur, 1987), Marcel Lesieur wrote "Turbulence is a dangerous topic which is often at the origin of serious fights in the scientific meetings devoted to it since it represents extremely different points of view, all of which have in common their complexity, as well as an inability to solve the problem." One point of view follows from adopting the Lagrangian frame of reference, the natural point of view for studying diffusive processes such as turbulence in the solar wind. This work develops Lagrangian statistics to quantify anisotropic MHD turbulence.

Anisotropy is introduced to a turbulent plasma by a macroscopic magnetic field[1], typically designated B_0, and measured with respect to the root-mean-square (RMS) fluctuations of the turbulent magnetic field B_{RMS}. In the solar wind, ion foreshock, and magnetosheath, ranges have been reported such that the macroscopic magnetic field is between one and 2.5 times the RMS fluctuations (Zimbardo et al., 2010). In Earth's plasma sheet the macroscopic magnetic field is on the order of two times the RMS fluctuations of the turbulent magnetic field ($B_0 \approx 2B_{\mathsf{RMS}}$) (Borovsky, 2005). In the magnetotail, observational data indicates that the magnetic field is stronger, between 3 and 5 times the RMS fluctuations (see table 1 of Zimbardo et al. (2010)). We examine a system with a moderately strong anisotropy caused by a macroscopic magnetic field of magnitude 3 times the average RMS magnetic field fluctuations. The observations from our simulations may reveal characteristics of the anisotropy due to the strongest macroscopic magnetic fields of the solar wind, or the weakest magnetic fields in the magnetotail.

Motivated by new experimental techniques developed over the last two decades, e.g. La Porta, Voth, Moisy, and Bodenschatz (2000); Mordant, Lévêque, and Pinton (2004); Xu, Bourgoin, Ouellette, Bodenschatz, et al. (2006); Biferale et al. (2008); Bourgoin, Pinton, and Volk (2014); Bourgoin and Xu (2014); Liot, Seychelles, et al. (2016); Liot, Gay, Salort, Bourgoin, and Chillà (2016); Lawson, Bodenschatz, Lalescu, and Wilczek (2018); Polanco, Vinkovic, Stelzenmuller, Mordant, and Bourgoin (2018); Lawson, Bodenschatz, Knutsen, Dawson, and Worth (2019), Lagrangian statistics of turbulent flows are attracting increasing attention. In oceanography and atmospheric science, Lagrangian measurements have a rich history, e.g. as discussed by Businger, Johnson, and Talbot (2006); LaCasce (2008a, 2008b); Fossette, Putman, Lohmann, Marsh, and Hays (2012); Aksamit, Sapsis, and Haller (2020). In space physics, the Cluster mission (Escoubet et al., 1997)

[1] In fundamental studies the macroscopic magnetic field is more often called a guide field or a mean field.

and the CubeSat project (Poghosyan & Golkar, 2017) have demonstrated that measurements made from multiple space-crafts will be feasible in the future.

Responding to the availability of high-quality measurements, high-resolution numerical simulations are enabling increasingly detailed studies of the dynamics of Lagrangian tracer particles, e.g. Yeung and Borgas (2004); Biferale et al. (2005); Buaria, Yeung, and Sawford (2016); Sawford and Yeung (2015); Bianchi, Biferale, Celani, and Cencini (2016); Schneide, Pandey, Padberg-Gehle, and Schumacher (2018). This explosion of work using Lagrangian tracer particles to explore the fundamental statistics of turbulence in neutral fluids has been summarized in several reviews, including S. Pope (1994); Wilson and Sawford (1996); Yeung (2002); Toschi and Bodenschatz (2009); Meneveau (2011) and a comprehensive review dedicated to two-particle dispersion, Salazar and Collins (2009).

The first program to investigate MHD turbulence from the Lagrangian point of view began over a decade ago as a collaboration between a group at the Max Planck Institute for Plasma Physics and a group at the Ruhr-Universität Bochum (Müller & Busse, 2007b; Busse et al., 2007; Müller & Busse, 2007a; Homann, Grauer, et al., 2007; Busse & Müller, 2008; Homann et al., 2009; Busse et al., 2010). That work was based on direct numerical simulations of three-dimensional incompressible homogeneous MHD turbulence. Here we revisit some of the fundamental results of those earlier studies, using new simulations at higher Reynolds number. We also expand on progress that has been made more recently to use Lagrangian statistics for anisotropic turbulence driven by convection and magnetoconvection (Pratt et al., 2017). We discuss further directions for future work.

2 Direct Numerical Simulations for Lagrangian single-particle diffusion and two-particle dispersion

To study diffusion and dispersion we produce simulations of statistically stationary, forced, homogeneous incompressible MHD turbulence. In each direct numerical simulation presented in this work, we solve the non-dimensional equations for incompressible magnetohydrodynamics:

$$\frac{\partial \boldsymbol{\omega}}{\partial t} - \nabla \times (\boldsymbol{v} \times \boldsymbol{\omega} + \boldsymbol{j} \times \boldsymbol{B}) = \hat{\nu} \nabla^2 \boldsymbol{\omega} + \boldsymbol{f}^{\omega} \ , \tag{1}$$

$$\frac{\partial \boldsymbol{B}}{\partial t} - \nabla \times (\boldsymbol{v} \times \boldsymbol{B}) = \hat{\eta} \nabla^2 \boldsymbol{B} + \boldsymbol{f}^{b} \ , \tag{2}$$

using a pseudospectral method in a three-dimensional rectangular simulation volume with periodic boundary conditions. These equations include the solenoidal velocity field $\boldsymbol{v}$, vorticity $\boldsymbol{\omega} = \nabla \times \boldsymbol{v}$, magnetic field $\boldsymbol{B}$, and current density $\boldsymbol{j} = \nabla \times \boldsymbol{B}$. Each of the quantities in eqs. (1) and (2) has been non-dimensionalized using relevant time and length scales, commonly referred to as Alfvénic units. Two dimensionless parameters, $\hat{\nu}$ and $\hat{\eta}$, appear in the equations. They derive from the kinematic viscosity ν and the magnetic diffusivity η. A fixed time-step and a low-storage third-order Runge–Kutta method (Williamson, 1980) are used for the time-integration. A static macroscopic magnetic field B_0 pointing in the positive z-direction may be imposed.

To maintain a statistically stationary turbulent steady state, both the vorticity and magnetic fields are forced on the largest scales of the simulation volume using a method that allows the largest scale motions of the system to evolve. This deterministic homogeneous method of forcing establishes a constant injection of energy at large scales (see Busse (2009) for a detailed discussion of this forcing method). In eqs. (1) and (2) forcing terms $\boldsymbol{f}^{\omega}$ and $\boldsymbol{f}^{b}$ are introduced. For the simulations in Table 1, these forcing terms are non-zero only for the wave-vector shell $1 \leq |\boldsymbol{k}| \leq 2.5$. The same amount of energy is injected into each forced mode according to

$$\boldsymbol{f}^{\omega}(\boldsymbol{k}, t) = \gamma_{f,\omega} \frac{\hat{\boldsymbol{\omega}}(\boldsymbol{k}, t)}{|\hat{\boldsymbol{\omega}}(\boldsymbol{k}, t)|^2} \ , \tag{3}$$

$$\boldsymbol{f}^b(\boldsymbol{k},t) \quad = \quad \gamma_{f,B}\frac{\hat{\boldsymbol{B}}(\boldsymbol{k},t)}{|\hat{\boldsymbol{B}}(\boldsymbol{k},t)|^2}\ . \tag{4}$$

The constants $\gamma_{f,\omega}$ and $\gamma_{f,B}$ regulate the energy injection rate, and are equal for the simulations in Table 1. Using homogeneous forcing, the cross helicity of the forced modes is maintained as a small non-zero value to prevent the emergence of states dominated by Elsässer positive (z^+) or negative (z^-) interactions, i.e. states where the MHD turbulent system becomes maximally imbalanced. Such a state can lead to a break-down of the non-linear energy cascade, e.g. as discussed in Biskamp (2003). In a system in quasi-stationary state, homogeneous forcing is expected to disturb the natural turbulent flow only mildly. This forcing method is distinct from those used by Busse et al. (2007); Homann, Grauer, et al. (2007); Busse and Müller (2008); Busse et al. (2010). Large-scale Alfvén waves are permitted by this forcing method and are observed in the simulations examined in this work.

Table 1 provides a summary of the fundamental parameters of the simulations we consider. Each simulation is performed on a grid of 1024^3 collocation points. In the table, we record the strength of the macroscopic magnetic field B_0 imposed in the z direction, as well as the root-mean-square of the magnetic fluctuations B_{RMS}, averaged over the simulation time. We measure length in units of the Kolmogorov microscale $\eta_{\mathsf{kol}} = (\hat{\nu}^3/\epsilon_{\mathrm{v}})^{1/4}$ and time in units of the Kolmogorov time-scale $\tau_\eta = (\hat{\nu}/\epsilon_{\mathrm{v}})^{1/2}$, where $\epsilon_{\mathrm{v}} = \hat{\nu}\langle\sum_{\boldsymbol{k}} \boldsymbol{k}^2\hat{\boldsymbol{v}}^2\rangle$ is the time-averaged rate of kinetic energy dissipation; the Kolmogorov microscales are the smallest length and time scales that characterize turbulent flows.

The Kolmogorov microscales define the resolution requirements for a direct numerical simulation (DNS). All of our simulations fulfill the classic criterion of S. B. Pope (2000); Yeung and Pope (1989) for a DNS, i.e. $k_{\max}\eta_{\mathsf{kol}} > 1.5$. This criterion has been widely used to evaluate whether homogeneous isotropic turbulence is sufficiently resolved (see also Yeung, Sreenivasan, and Pope (2018) for a recent study of the effect of resolution on homogeneous isotropic turbulence). For reference, the Eulerian kinetic and magnetic energy spectra for the simulations described in Table 1 are provided in Figure 1.

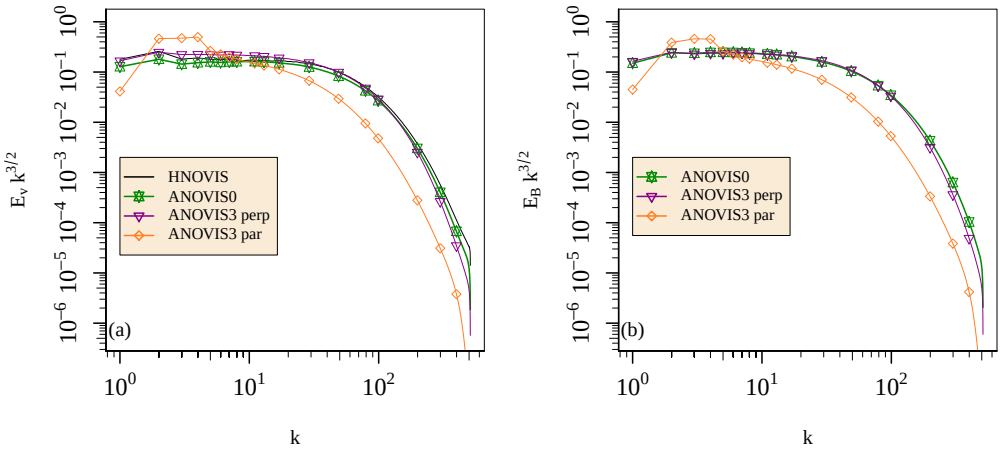

Figure 1. Energy spectra for the simulations in Table 1 (a) kinetic energy spectra, and (b) magnetic energy spectra. These spectra are compensated by $k^{3/2}$.

For simulations of MHD turbulence that are anisotropic because of the effect of a mean magnetic field, a box that is elongated in the z-direction has been used in many

earlier works, including for example Mason, Cattaneo, and Boldyrev (2006). To determine the necessary elongation of the simulation volume in the z-direction, we consider the correlation length of the velocity field in each direction. We measure a correlation length of the velocity field in the z-direction, $L_{\mathsf{c},\parallel}$, that is larger than in the x and y directions, in agreement with previous studies, e.g. Chandran (2008); Boldyrev (2005); Cho, Lazarian, and Vishniac (2002). To accommodate this larger $L_{\mathsf{c},\parallel}$ within our simulation volume, we elongate the simulation volume in the z-direction, so that the condition on the box length in the z-direction $L_z \gg L_{\mathsf{c},\parallel}$ is satisfied. The elongation of the simulation box, as measured by the ratio of the box length in the z-direction to the box length in the x-direction, L_z/L_x, is listed in the table for each simulation. The simulation volume has sides of length $L_x = L_y = 2\pi$ in the perpendicular directions.

2.1 Lagrangian tracer particles

For the simulations in Table 1, the positions of Lagrangian tracer particles are initialized in a homogeneous random distribution at a time when the turbulent flow is in a statistically stationary steady state. The total number of particles in each simulation is $\mathsf{n_p} \approx 8.3$ million. This is a high density of tracer particles, comparable to earlier works (Müller & Busse, 2007b; Busse et al., 2007; Müller & Busse, 2007a; Homann, Grauer, et al., 2007; Busse & Müller, 2008; Homann et al., 2009; Busse et al., 2010). The number of Lagrangian tracer particles that we use produces statistics that are well-resolved in space.

At each time step the particle velocities are interpolated from the instantaneous Eulerian velocity field using a tricubic polynomial interpolation scheme (for a clear analysis of the impact of the interpolation scheme on Lagrangian statistics, see Homann, Dreher, and Grauer (2007)). Particle positions are calculated by numerical integration of the equations of motion using a low-storage third-order Runge–Kutta method identical to that used for the Eulerian fields. Each simulation is run for a sufficient time that Lagrangian particle pair-separations exhibit a diffusive trend. This length of time is approximately 400 τ_η, an amount of time that allows the particles in our hydrodynamic simulations (HNOVIS and HPUFF) to cross the simulation volume approximately once, on average. Because the Lagrangian tracer particles do not cross the simulation volume multiple times, the periodic boundary conditions have no observed effect on the statistics produced.

2.2 Reynolds number for anisotropic MHD turbulence

For an isotropic system with $B_0 = 0$, we define the Reynolds number in the standard way as

$$\mathsf{Re} = \langle \mathsf{E_v}^{1/2} \mathsf{L_E} \rangle / \hat{\nu} \ , \tag{5}$$

from the kinetic energy $\mathsf{E_v}$, a characteristic length scale $\mathsf{L_E}$, and the viscosity $\hat{\nu}$. For statistically homogeneous isotropic turbulent flows, $\mathsf{L_E}$ is commonly defined as a dimensional estimate of the size of the largest eddies, $\mathsf{L_E} = {\mathsf{E_v}}^{3/2}/\epsilon_\mathrm{v}$, using ϵ_v, the rate of kinetic energy dissipation. The calculated value of this length scale $\mathsf{L_E}$ is included in Table 1 for each of our simulations.

To compare isotropic and anisotropic turbulent flows, we use a more basic definition of the Reynolds number (see chapter 6.1.2 of S. B. Pope (2000))

$$\mathsf{Re} = c \ (\eta_\mathsf{kol}/\mathsf{L_F})^{-4/3} \ . \tag{6}$$

This definition requires knowledge of the forcing length scale $\mathsf{L_F}$, and a constant c. Our method of forcing affects a minimum length scale

$$\mathsf{L_F} = 2\pi/k_{f,\mathsf{max}} = 2\pi/3 \ . \tag{7}$$

We determine the constant c by comparison with the definition of the Reynolds number in the isotropic case given in eq. (5). The Reynolds number is calculated in this way for simulation ANOVIS3 in Table 1. The magnetic Reynolds number is defined from the Reynolds number and the magnetic Prandtl number, i.e. $\mathsf{Re_m} = \mathsf{Pr_m Re}$. In all simulations in this work, the magnetic Prandtl number $\mathsf{Pr_m} = 1$ so that the magnetic Reynolds number is equal to the Reynolds number.

3 Single-particle diffusion and two-particle dispersion in MHD turbulence

Perhaps the most fundamental result from studies of Lagrangian statistics in MHD turbulence is a comparison of single-particle diffusion and two-particle dispersion. While single-particle diffusion exhibits the same essential behavior in hydrodynamic turbulence and MHD turbulence, two-particle relative dispersion in MHD turbulence differs significantly from the hydrodynamic behavior (Busse et al., 2007). This is a significant observation, because single particle statistics are heavily impacted by the largest scales; two-particle statistics effectively limit contributions from the largest scales of the flow. A single-particle diffusion curve follows the evolution of the average square distance a particle has moved from its initial position, represented by $\langle \xi^2 \rangle$. We compare single-particle diffusion curves for two isotropic turbulence flows: in hydrodynamic turbulence (simulation HNOVIS) and in MHD turbulence (simulation ANOVIS0), see Figure 2. These two diffusion curves exhibit nearly identical behavior. This figure also includes the curves for an anisotropic MHD turbulence simulation, ANOVIS3, which is significantly different from either isotropic case. The results from ANOVIS3 have been split into diffusion in the direction of the mean magnetic field, and diffusion in the direction perpendicular to the mean magnetic field. Diffusion in both these distinct directions takes a characteristically similar shape. Each of the curves in Figure 2 exhibits a clear ballistic scaling as t^2 at early times, and has entered a diffusive regime with scaling close to t at late times. At early intermediate times, both the diffusion parallel and perpendicular to the mean magnetic field grow more slowly in anisotropic MHD than in either isotropic simulation. This slow-down is larger in the direction parallel to the mean magnetic field. During the later part of the intermediate time period, the separation process accelerates; diffusion then slows as the diffusive regime is reached. These observations agree with results first reported in Busse and Müller (2008) and Busse (2009).

The velocity autocorrelation function has a differential relation to diffusion; these are Green–Kubo relations, e.g. as discussed in Alder, Gass, and Wainwright (1970); Dubbeldam, Ford, Ellis, and Snurr (2009). Because of this, the velocity autocorrelation function is typically used to shed new light on diffusion by providing information about the relaxation of fluctuations over long times and distances. For Brownian motion, the velocity autocorrelation function is fit well by a single decaying exponential. A single decaying exponential has also been shown to be a good fit for hydrodynamic turbulence in both experimental and numerical studies (Sato & Yamamoto, 1987; Yeung & Pope, 1989). A single decaying exponential is an excellent fit for the velocity autocorrelation function of simulation HNOVIS (see Figure 3). However for the MHD simulations ANOVIS0 and ANOVIS3, it is not clear whether a single decaying exponential is a reasonable model. Isotropic MHD turbulence leads to a swifter overall decay of the velocity autocorrelation function than hydrodynamic turbulence. In anisotropic MHD turbulence, this swift decay is further exaggerated, fundamentally changing the initial shape of the decay of the velocity autocorrelation function so that a decaying exponential produces a poor fit. In the anisotropic case, large scale Alfvénic fluctuations are clearly visible in the velocity autocorrelation function. The characteristic time of decay for the velocity autocorrelation function is smaller in the anisotropic case than in the isotropic case. In the direction aligned with the mean magnetic field this decay time is slightly shorter than in the direction perpendicular. Small-scale fluctuations in the velocity are therefore more

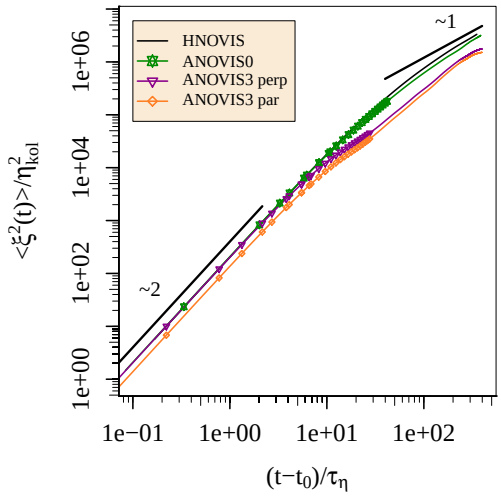

Figure 2. Evolution of mean-square distance from the initial position for the three simulations described in Table 1. The mean-square distance for the anisotropic MHD simulation ANOVIS3 is separated into distances parallel and perpendicular to the mean magnetic field. Each curve is produced from the average of at least 4 independent initial times.

probable in the direction perpendicular to the magnetic field. Over long times, the absolute diffusion parallel to the mean magnetic field is therefore smaller because of the different prevalence in velocity fluctuations.

For two-particle dispersion, Busse et al. (2007) find considerable differences between isotropic hydrodynamic turbulence and isotropic MHD turbulence. We examine pairs of particles that are initially separated by $2\eta_{\mathrm{kol}}$, the smallest initial separation that is resolved by our grid (see Figure 4). Each of these curves exhibits a clear ballistic scaling as t^2 at early times, and has entered a diffusive regime at late times. In the diffusive regime of these dispersion curves, a mildly superdiffusive slope is evident. The anisotropic MHD simulation ANOVIS3 is the most superdiffusive with a slope near three at these late times. The dispersion curves of simulation ANOVIS3 also show an oscillation that we attribute to large-scale Alfvénic fluctuations. We find that the rate of dispersion is slower for MHD turbulence than for hydrodynamic turbulence. This rate of dispersion first slows down at early intermediate times, as the dispersion curves depart from ballistic scaling. The slow-down is more significant for the anisotropic MHD simulation ANOVIS3 than for the isotropic MHD simulation ANOVIS0. This slow-down feature that is common between isotropic and anisotropic MHD simulations may be explained as an effect of the local, fluctuating magnetic field. This field appears to be sufficient to produce a degree of anisotropy in the relative dispersion process, even in a globally isotropic simulation.

4 Direct Numerical Simulations for Lagrangian many-particle dispersion

To examine many-particle dispersion, we conduct a separate series of simulations that use a significantly different initial set-up of Lagrangian tracer particles. The positions of the Lagrangian tracer particles are initialized into spherical volumes of a specified size and density of tracer particles, henceforth called *droplets*. The droplets are homogeneously and randomly distributed throughout the simulation volume at a time when

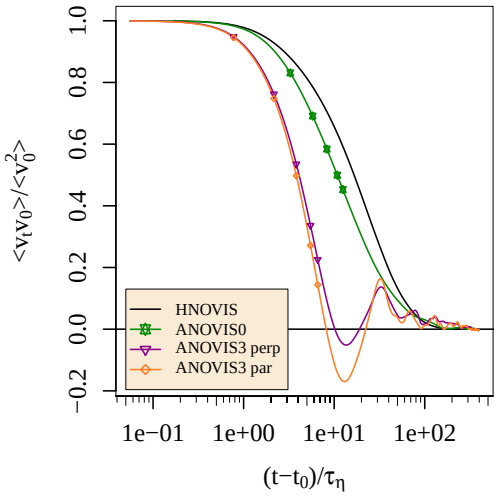

Figure 3. Velocity autocorrelation function for the three simulations described in Table 1. The velocity autocorrelation function for the anisotropic MHD simulation ANOVIS3 is separated into velocities in the direction parallel and perpendicular to the mean magnetic field. Each curve is produced from the average of at least 4 independent initial times.

the turbulent flow is in a statistically stationary steady state. A visualization of such a droplet dispersing is shown in Figure 5. Simulations using this initial droplet set-up for Lagrangian particles were published in Pratt et al. (2017) for a study of convection, and a similar initial set-up was used to study Navier–Stokes turbulence in Bianchi et al. (2016). Each simulation described in Table 2 has this initial set-up, and a total number of tracer particles of $\mathsf{n_p} \approx 4.5$ million.

For the simulations in Table 2, a stochastic forcing method, as described by Eswaran and Pope (1988b, 1988a); Busse (2009), is used. For simulations HPUFF and APUFF0, the forcing terms are non-zero only for the wave-vector shell $1 \leq |\boldsymbol{k}| \leq 2.5$. For simulation APUFF3, this forcing wave-vector shell is shifted to $2.5 \leq |\boldsymbol{k}| \leq 3.5$; this adjustment was made because forcing wave-vectors in the lower k shell in combination with the mean magnetic field was found to lead to a build-up of energy at large scales, significantly changing the energy spectra. For reference, the Eulerian kinetic and magnetic energy spectra of the simulations described in Table 2 are provided in Figure 6. As with the previous series of simulations, large-scale Alfvénic fluctuations are permitted by the stochastic forcing method and are observed in our simulations. Aside from the different initial set-up of Lagrangian tracer particles and the use of a stochastic forcing method, the simulations in Table 2 follow a similar set-up to the simulations in Table 1.

5 Many-particle dispersion in MHD turbulence

Lagrangian statistics are known to be sensitive to extreme events in the fluctuating turbulent fields, e.g. Yeung and Borgas (2004); Boffetta and Sokolov (2002). In Pratt et al. (2017), we developed an analysis using the convex hull to calculate the extremes of dispersion of a group of many Lagrangian tracer particles. The simplest diagnostic resulting from this approach is the maximal ray internal to a convex hull. For a group of particles G, the maximal ray can be calculated:

$$r = \max_{i,j \in G} \sqrt{(x_i - x_j)^2 + (y_i - y_j)^2 + (z_i - z_j)^2} \; . \tag{8}$$

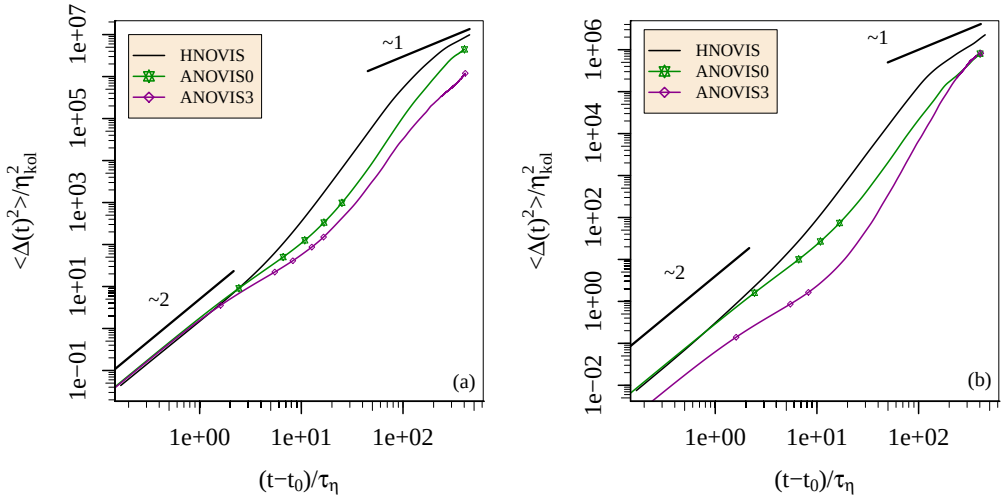

Figure 4. Evolution of mean-square separation of pairs of Lagrangian tracer particles in homogeneous isotropic hydrodynamic turbulence (simulation HNOVIS), homogeneous isotropic MHD turbulence (simulation ANOVIS0), and homogeneous anisotropic MHD turbulence (simulation ANOVIS3). The behavior for pairs with an initial separation of $2\eta_{\text{kol}}$ is shown (a) for particles initially separated in the direction perpendicular to the mean magnetic field and separation distance measured perpendicular to the field, and (b) for particles initially separated in the direction parallel to the mean magnetic field, and separation distance measured aligned with the mean magnetic field.

This measure of separation is based on pairs of particles within the droplet that are furthest apart at a given point in time, so that it always is defined as the largest extent of dispersion of the group. Thus different particles may be used to determine the maximal ray as the convex hull evolves in time; in contrast, two-particle dispersion always considers a fixed pair of particles. The maximal ray evolves with similar ballistic, intermediate, and diffusive phases to two-particle dispersion (see Figure 7). However, because it measures the extreme of dispersion, during the initial short ballistic regime the maximal ray dispersion curve grows slightly more quickly than t^2. In the intermediate regime, we observe that even the extremes of dispersion are slowed by the presence of magnetic fields, with dispersion in the anisotropic MHD simulation APUFF3 growing more slowly than in the isotropic case APUFF0. This has interesting overlap with the earlier observation (Busse, 2009) that intermittency in particle accelerations is lower in isotropic MHD turbulence than in isotropic hydrodynamic turbulence, and lower still in anisotropic MHD turbulence. The extremes of dispersion, not just the averages, are suppressed by the anisotropy of the magnetic fluctuations.

In Pratt et al. (2017), we used the surface area s and volume v of the convex hull surrounding the Lagrangian tracer particles to quantify the anisotropy in each simulation. For a perfect sphere, the non-dimensional ratio $s/v^{2/3}$ takes a value of $(36\pi)^{1/3} \approx 4.8$; for an anisotropic shape like a pancake or needle, this ratio will be larger. The magnitude of this ratio, compared with 4.8, indicates how anisotropic the convex hull around a group of Lagrangian tracer particles is. During intermediate times corresponding to the early intermediate range of time scales, the anisotropy ratio grows dramatically for all simulations. For the hydrodynamic simulation HPUFF, this period lasts between approximately τ_η and $8\tau_\eta$; for the MHD simulations this period lasts more than twice as

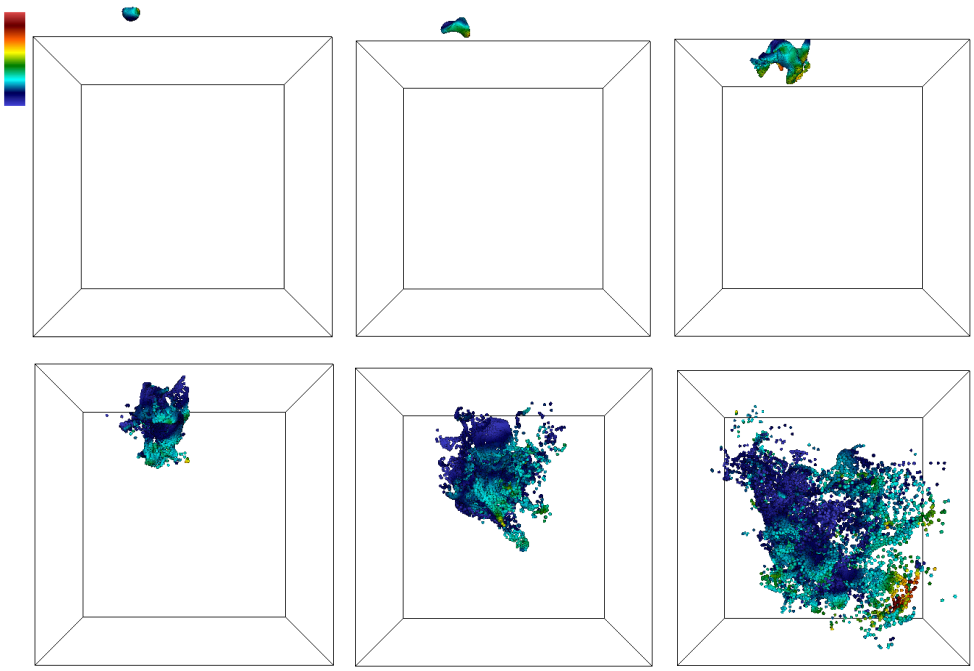

Figure 5. Diffusion of a single droplet with initial diameter $14\eta_{\mathsf{kol}}$, composed of approximately 16 thousand Lagrangian tracer particles, in simulation HPUFF. The series of 6 snapshots documents the dispersion of the particles over approximately 40 τ_η. Particles are colored by the kinetic energy of the flow.

long, between approximately τ_η and $20\tau_\eta$. The time of the peak correlates with the acceleration of dispersion in the pair dispersion curves or the maximal ray curves for each of these simulations. After this rise in the anisotropy ratio, it falls to lower levels (see Figure 8), eventually indicating isotropic growth of the droplets in the early diffusive regime, with a shape near spherical. Many works have argued that anisotropy in MHD turbulence is length scale dependent, e.g. as discussed by Cho and Vishniac (2000); Schekochihin, Cowley, and Yousef (2008); Verdini, Grappin, Hellinger, Landi, and Müller (2015). Figure 8 demonstrates that anisotropy is time-scale dependent, from the Lagrangian point of view. In addition, the evolution of the anisotropy ratio reveals a new structure to that scale dependence.

The anisotropy ratio becomes larger in both isotropic and anisotropic MHD than in our hydrodynamic simulation. It is also slightly larger in isotropic MHD turbulence than in anisotropic MHD turbulence. However the strong overlap of the shaded regions in Figure 8, which indicate one standard deviation above and below the average line, indicate that this difference between the average lines for these simulations is not statistically significant. The difference in the anisotropy ratio between hydrodynamic turbulence and MHD turbulence is clearly statistically significant. A comparison between panels (a) and (b) of this figure demonstrates that, for initially smaller groups of particles, a larger anisotropy ratio is achieved. This also gives an indication that intermittency is different on different length scales of a turbulent flow.

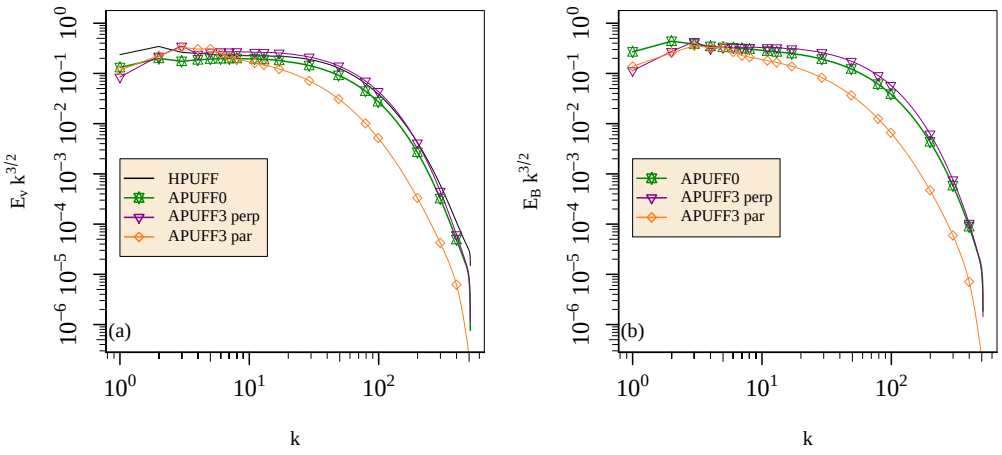

Figure 6. Energy spectra for the simulations in Table 2 (a) kinetic energy spectra, and (b) magnetic energy spectra. These spectra are compensated by $k^{3/2}$.

6 Summary and Discussion

Lagrangian tracer particles provide a powerful tool for quantifying diffusion and dispersion in MHD turbulence. In the simulations presented here, we have confirmed that single-particle diffusion curves are similar for isotropic hydrodynamic and magnetohydrodynamic turbulence. However, for anisotropic MHD turbulence the single-particle diffusion curves exhibit characteristic differences; they show slower diffusion at intermediate separation times. Two-particle dispersion curves for isotropic MHD turbulence have clear differences from isotropic hydrodynamic turbulence. Anisotropic MHD turbulence makes those differences larger. We obtain these results from three simulations that have identical resolution and closely comparable Reynolds numbers and general set-up. These simulations have higher Reynolds numbers, and a weaker mean magnetic field than earlier works (Busse et al., 2007; Busse & Müller, 2008; Busse, 2009), but our findings agree in a broad sense.

Single-particle diffusion and two-particle dispersion curves provide critical information, however they do not provide a complete picture of transport processes for anisotropic MHD turbulence. We therefore extend our examination of dispersion using the novel many-particle methods developed in Pratt et al. (2017). This is a new application of statistical methods originally developed to examine anisotropy in convection simulations. These methods use a convex hull algorithm to describe the outer surface of a group of many particles that are initially tightly packed into a spherical configuration, which we call a droplet. The maximal ray, which represents the extremes of dispersion, is found to follow a pattern similar to the two-particle dispersion: the speed of dispersion can be ordered with hydrodynamic turbulence producing the fastest dispersion, then isotropic MHD turbulence, and then anisotropic MHD turbulence. Thus MHD turbulence can be shown to suppress even the extremes of particle dispersion. When we examine the anisotropy ratio for groups of many Lagrangian tracer particles, both isotropic and anisotropic MHD turbulence are more anisotropic than hydrodynamic turbulence. The anisotropy ratio clearly reveals the dependence of anisotropy on separation time scales, a concept that translates to length-scale dependent anisotropy, which has been observed in the Eulerian frame of reference.

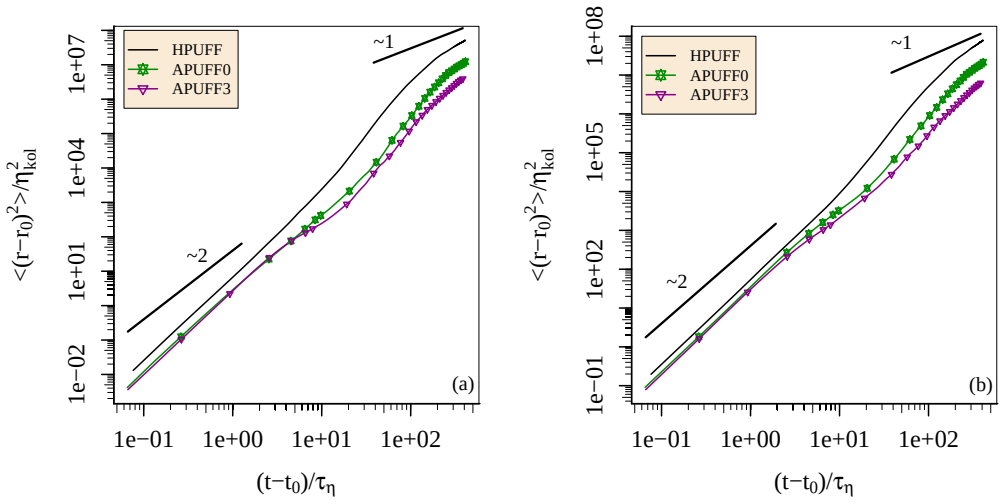

Figure 7. Evolution of mean-square maximal ray r of the droplets for the simulations described in Table 2. Droplets have identical initial particle density, and an initial diameter of (a) $4\eta_{\text{kol}}$, and (b) $14\eta_{\text{kol}}$.

In order to fully understand how magnetic fields affect MHD turbulence and anisotropy, further development of Lagrangian statistics is needed. One aspect in particular that would be helpful to clarify transport processes is the analysis of particle trajectories in MHD turbulence; studies of particle trajectories in neutral fluid turbulence have produced interesting results in recent years (Ouellette & Gollub, 2007; Xu et al., 2007; Choi et al., 2010; Siu & Taylor, 2011; Bos et al., 2015). Quantifying the trajectories involves calculating the curvature and torsion that a particle experiences along its path. To better understand these trajectories, studies of the extremes of acceleration (Homann, Grauer, et al., 2007) need to be further developed for anisotropic MHD turbulence. Intriguing experimental results for the acceleration PDF of neutral-fluid turbulence (e.g. Mordant, Crawford, and Bodenschatz (2004); Liot, Gay, et al. (2016)) make it likely that there is a great deal more to understand about MHD turbulence through the peculiar behavior of the Lagrangian acceleration. In addition, studies of anisotropic MHD turbulence are often based on relatively few simulations, and therefore do not reveal the role of the mean magnetic field in generating anisotropy and changing transport properties. A larger range of anisotropic simulations needs to be studied in conjunction so that the influence of a mean magnetic field can be established. These areas of study are included in our ongoing and planned work.

Acknowledgments

This material is based upon work supported by the National Science Foundation under Grant No. 1907876. Simulations were performed on the Konrad and Gottfried computer systems of the Norddeutsche Verbund zur Förderung des Hoch- und Höchstleistungsrechnens (HLRN) by the project bep00051 “Lagrangian studies of incompressible turbulence in plasmas”.

In accordance with the Enabling FAIR data Project guidelines, simulation data associated with this work is made permanently available on the author’s FigShare repos-

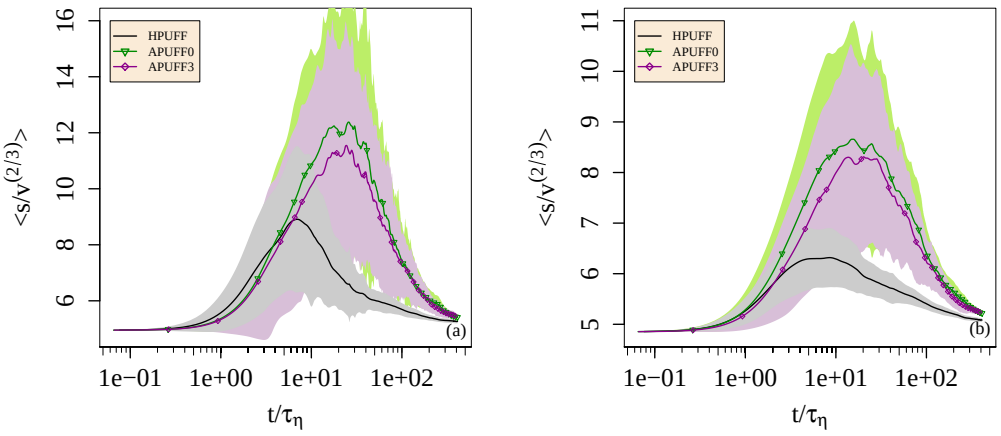

Figure 8. Average anisotropy ratio for the simulations described in Table 2, for droplets with (a) an initial diameter of $4\eta_{\mathsf{kol}}$, and (b) an initial diameter of $14\eta_{\mathsf{kol}}$. The density of particles in both sizes of droplet is the same. A shaded area indicating one standard deviation above and below each line is provided.

itory `https://figshare.com/authors/Jane_Pratt/2136082` (Pratt et al., 2020c, 2020e, 2020d, 2020b, 2020a).

References

Aksamit, N. O., Sapsis, T., & Haller, G. (2020). Machine-learning mesoscale and submesoscale surface dynamics from Lagrangian ocean drifter trajectories. *J. Phys. Oceanogr.*, *50*(5), 1179–1196.

Alder, B., Gass, D., & Wainwright, T. (1970). Studies in molecular dynamics. viii. the transport coefficients for a hard-sphere fluid. *J. Chem. Phys.*, *53*(10), 3813–3826.

Bianchi, S., Biferale, L., Celani, A., & Cencini, M. (2016). On the evolution of particle-puffs in turbulence. *Eur. J. Mech. B Fluids*, *55*, 324–329.

Biferale, L., Bodenschatz, E., Cencini, M., Lanotte, A. S., Ouellette, N. T., Toschi, F., & Xu, H. (2008). Lagrangian structure functions in turbulence: A quantitative comparison between experiment and direct numerical simulation. *Phys. Fluids*, *20*(6), 065103.

Biferale, L., Boffetta, G., Celani, A., Devenish, B., Lanotte, A., & Toschi, F. (2005). Lagrangian statistics of particle pairs in homogeneous isotropic turbulence. *Phys. Fluids*, *17*(11), 115101.

Biskamp, D. (2003). *Magnetohydrodynamic turbulence*. Cambridge University Press.

Boffetta, G., & Sokolov, I. (2002). Relative dispersion in fully developed turbulence: the Richardson's law and intermittency corrections. *Phys. Rev. Lett.*, *88*(9), 094501.

Boldyrev, S. (2005). On the spectrum of magnetohydrodynamic turbulence. *ApJ Lett.*, *626*(1), L37.

Borovsky, J. E. (2005). A model for the mhd turbulence in the earth's plasma sheet: Building computer simulations. In *Multiscale processes in the earth's magnetosphere: From interball to cluster* (pp. 217–253). Springer.

Bos, W. J., Kadoch, B., & Schneider, K. (2015). Angular statistics of Lagrangian trajectories in turbulence. *Phys. Rev. Lett.*, *114*(21), 214502.

Bourgoin, M., Pinton, J.-F., & Volk, R. (2014). Lagrangian methods in experimental fluid mechanics. *Modeling Atmospheric and Oceanic Flows: Insights from Laboratory Experiments and Numerical Simulations*, 277–296.

Bourgoin, M., & Xu, H. (2014). Focus on dynamics of particles in turbulence. *New J. Phys.*, *16*(8), 085010.

Buaria, D., Yeung, P., & Sawford, B. (2016). Lagrangian statistics of turbulent dispersion from 8192^3 direct numerical simulation of isotropic turbulence. In *APS Meeting Abstracts.*

Businger, S., Johnson, R., & Talbot, R. (2006). Scientific insights from four generations of Lagrangian smart balloons in atmospheric research. *Bull. Am. Meteorol. Soc.*, *87*(11), 1539–1554.

Busse, A. (2009). *Lagrangesche statistische eigenschaften hydrodynamischer und magnetohydrodynamischer turbulenz* (Doctoral dissertation, Universität Bayreuth). University of Bayreuth, Faculty of Mathematics, Physics and Computer Sciences.

Busse, A., & Müller, W.-C. (2008). Diffusion and dispersion in magnetohydrodynamic turbulence: The influence of mean magnetic fields. *Astronomische Nachrichten: Astronomical Notes*, *329*(7), 714–716.

Busse, A., Müller, W.-C., & Gogoberidze, G. (2010). Lagrangian frequency spectrum as a diagnostic for magnetohydrodynamic turbulence dynamics. *Phys. Rev. Lett.*, *105*(23), 235005.

Busse, A., Müller, W.-C., Homann, H., & Grauer, R. (2007). Statistics of passive tracers in three-dimensional magnetohydrodynamic turbulence. *Phys. Plasmas*, *14*(12), 122303.

Chandran, B. D. (2008). Strong anisotropic MHD turbulence with cross helicity. *ApJ.*, *685*(1), 646.

Cho, J., Lazarian, A., & Vishniac, E. T. (2002). Simulations of magnetohydrodynamic turbulence in a strongly magnetized medium. *ApJ*, *564*(1), 291.

Cho, J., & Vishniac, E. T. (2000). The anisotropy of magnetohydrodynamic Alfvénic turbulence. *ApJ*, *539*(1), 273.

Choi, Y., Park, Y., & Lee, C. (2010). Helicity and geometric nature of particle trajectories in homogeneous isotropic turbulence. *Int. J. Heat Fluid Fl.*, *31*(3), 482–487.

Dubbeldam, D., Ford, D. C., Ellis, D. E., & Snurr, R. Q. (2009). A new perspective on the order-n algorithm for computing correlation functions. *Molecular Simulation*, *35*(12-13), 1084–1097.

Escoubet, C., Schmidt, R., & Goldstein, M. (1997). Cluster-science and mission overview. In *The Cluster and Phoenix missions* (pp. 11–32). Springer.

Eswaran, V., & Pope, S. (1988a). Direct numerical simulations of the turbulent mixing of a passive scalar. *Phy. Fluids*, *31*(3), 506–520.

Eswaran, V., & Pope, S. B. (1988b). An examination of forcing in direct numerical simulations of turbulence. *Computers & Fluids*, *16*(3), 257–278.

Fossette, S., Putman, N. F., Lohmann, K. J., Marsh, R., & Hays, G. C. (2012). A biologist's guide to assessing ocean currents: a review. *Mar. Ecol. Prog. Ser.*, *457*, 285–301.

Homann, H., Dreher, J., & Grauer, R. (2007). Impact of the floating-point precision and interpolation scheme on the results of dns of turbulence by pseudo-spectral codes. *Comput. Phys. Commun.*, *177*(7), 560–565.

Homann, H., Grauer, R., Busse, A., & Müller, W.-C. (2007). Lagrangian statistics of Navier–Stokes and MHD turbulence. *J. Plasma Phys.*, *73*(6), 821–830.

Homann, H., Kamps, O., Friedrich, R., & Grauer, R. (2009). Bridging from eulerian to Lagrangian statistics in 3d hydro-and magnetohydrodynamic turbulent flows. *New J. Phys.*, *11*(7), 073020.

LaCasce, J. (2008a). Lagrangian statistics from oceanic and atmospheric observations. In *Transport and mixing in geophysical flows* (pp. 165–218). Springer.

LaCasce, J. (2008b). Statistics from Lagrangian observations. *Prog. Oceanogr.*, *77*(1), 1–29.

La Porta, A., Voth, G. A., Moisy, F., & Bodenschatz, E. (2000). Using cavitation to measure statistics of low-pressure events in large-reynolds-number turbulence. *Phys. Fluids*, *12*(6), 1485–1496.

Lawson, J. M., Bodenschatz, E., Knutsen, A. N., Dawson, J. R., & Worth, N. A. (2019). Direct assessment of kolmogorov's first refined similarity hypothesis. *Phys. Rev. Lett*, *4*(2), 022601.

Lawson, J. M., Bodenschatz, E., Lalescu, C. C., & Wilczek, M. (2018). Bias in particle tracking acceleration measurement. *Exp. Fluids*, *59*(11), 172.

Lesieur, M. (1987). *Turbulence in fluids: stochastic and numerical modelling.* Nijhoff Boston, MA.

Liot, O., Gay, A., Salort, J., Bourgoin, M., & Chillà, F. (2016). Inhomogeneity and Lagrangian unsteadiness in turbulent thermal convection. *Phys. Rev. Fluids*, *1*(6), 064406.

Liot, O., Seychelles, F., Zonta, F., Chibbaro, S., Coudarchet, T., Gasteuil, Y., ... Chillà, F. (2016). Simultaneous temperature and velocity Lagrangian measurements in turbulent thermal convection. *J. Fluid Mech.*, *794*, 655–675.

Mason, J., Cattaneo, F., & Boldyrev, S. (2006). Dynamic alignment in driven magnetohydrodynamic turbulence. *Phys. Rev. Lett.*, *97*(25), 255002.

Meneveau, C. (2011). Lagrangian dynamics and models of the velocity gradient tensor in turbulent flows. *Annu. Rev. Fluid Mech*, *43*, 219–245.

Mordant, N., Crawford, A. M., & Bodenschatz, E. (2004). Three-dimensional structure of the Lagrangian acceleration in turbulent flows. *Phys. Rev. Lett.*, *93*(21), 214501.

Mordant, N., Lévêque, E., & Pinton, J.-F. (2004). Experimental and numerical study of the Lagrangian dynamics of high reynolds turbulence. *New J. Phys.*, *6*(1), 116.

Müller, W.-C., & Busse, A. (2007a). Diffusion and dispersion of passive tracers: Navier-stokes vs. mhd turbulence. *EPL*, *78*(1), 14003.

Müller, W.-C., & Busse, A. (2007b). Recent developments in the theory of magnetohydrodynamic turbulence. In *AIP conference proceedings* (Vol. 932, pp. 52–57).

Ouellette, N. T., & Gollub, J. P. (2007). Curvature fields, topology, and the dynamics of spatiotemporal chaos. *Phys. Rev. Lett.*, *99*(19), 194502.

Poghosyan, A., & Golkar, A. (2017). Cubesat evolution: Analyzing cubesat capabilities for conducting science missions. *Prog. Aerosp. Sci.*, *88*, 59–83.

Polanco, J. I., Vinkovic, I., Stelzenmuller, N., Mordant, N., & Bourgoin, M. (2018). Relative dispersion of particle pairs in turbulent channel flow. *Int. J. Heat Fluid Fl.*, *71*, 231–245.

Pope, S. (1994). Lagrangian PDF methods for turbulent flows. *Annu. Rev. Fluid Mech*, *26*(1), 23–63.

Pope, S. B. (2000). *Turbulent flows.* Cambridge University Press.

Pratt, J., Busse, A., & Müller, W. C. (2020a). *Average anisotropy ratio for anisotropic mhd turbulence.* FigShare. doi: https://doi.org/10.6084/m9.figshare.12323822.v1

Pratt, J., Busse, A., & Müller, W. C. (2020b). *Maximal ray for a droplet of many particles dispersing in anisotropic mhd turbulence.* FigShare. doi: https://doi.org/10.6084/m9.figshare.12323813.v1

Pratt, J., Busse, A., & Müller, W. C. (2020c). *Single particle diffusion in anisotropic mhd turbulence.* FigShare. doi: https://doi.org/10.6084/m9.figshare.12323732.v1

Pratt, J., Busse, A., & Müller, W. C. (2020d). *Two-particle dispersion in anisotropic mhd turbulence.* FigShare. doi: https://doi.org/10.6084/m9.figshare.12323771.v1

Pratt, J., Busse, A., & Müller, W. C. (2020e). *Velocity autocorrelation function in anisotropic mhd turbulence.* FigShare. doi: https://doi.org/10.6084/m9.figshare.12323747.v1

Pratt, J., Busse, A., Müller, W. C., Watkins, N., & Chapman, S. C. (2017). Extreme-value statistics from Lagrangian convex hull analysis for homogeneous turbulent Boussinesq convection and MHD convection. *New J. Phys.*, *19*(6), 065006.

Salazar, J. P., & Collins, L. R. (2009). Two-particle dispersion in isotropic turbulent flows. *Annu. Rev. Fluid Mech*, *41*, 405–432.

Sato, Y., & Yamamoto, K. (1987). Lagrangian measurement of fluid-particle motion in an isotropic turbulent field. *J. Fluid Mech.*, *175*, 183–199.

Sawford, B. L., & Yeung, P. (2015). Direct numerical simulation studies of Lagrangian intermittency in turbulence. *Phys. Fluids*, *27*(6), 065109.

Schekochihin, A. A., Cowley, S. C., & Yousef, T. A. (2008). MHD turbulence: Nonlocal, anisotropic, nonuniversal? In *Iutam symposium on computational physics and new perspectives in turbulence* (pp. 347–354).

Schneide, C., Pandey, A., Padberg-Gehle, K., & Schumacher, J. (2018). Probing turbulent superstructures in rayleigh-bénard convection by Lagrangian trajectory clusters. *Phys. Rev. Lett*, *3*(11), 113501.

Siu, Y., & Taylor, A. (2011). Particle capture by turbulent recirculation zones measured using long-time Lagrangian particle tracking. *Exp. Fluids*, *51*(1), 95–121.

Toschi, F., & Bodenschatz, E. (2009). Lagrangian properties of particles in turbulence. *Annu. Rev. Fluid Mech*, *41*, 375–404.

Verdini, A., Grappin, R., Hellinger, P., Landi, S., & Müller, W. C. (2015). Anisotropy of third-order structure functions in MHD turbulence. *ApJ*, *804*(2), 119.

Williamson, J. H. (1980). Low-storage Runge-Kutta schemes. *J. Comput. Phys.*, *35*(1), 48 - 56. doi: DOI:10.1016/0021-9991(80)90033-9

Wilson, J. D., & Sawford, B. L. (1996). *Review of Lagrangian stochastic models for trajectories in the turbulent atmosphere.* Springer.

Xu, H., Bourgoin, M., Ouellette, N. T., Bodenschatz, E., et al. (2006). High order Lagrangian velocity statistics in turbulence. *Phys. Rev. Lett.*, *96*(2), 024503.

Xu, H., Ouellette, N. T., & Bodenschatz, E. (2007). Curvature of Lagrangian trajectories in turbulence. *Phys. Rev. Lett.*, *98*(5), 050201.

Yeung, P. (2002). Lagrangian investigations of turbulence. *Annu. Rev. Fluid Mech*, *34*(1), 115–142.

Yeung, P., & Borgas, M. S. (2004). Relative dispersion in isotropic turbulence. Part 1. Direct numerical simulations and Reynolds-number dependence. *J. Fluid Mech.*, *503*, 93–124.

Yeung, P., & Pope, S. (1989). Lagrangian statistics from direct numerical simulations of isotropic turbulence. *J. Fluid Mech.*, *207*, 531–586.

Yeung, P., Sreenivasan, K., & Pope, S. (2018). Effects of finite spatial and temporal resolution in direct numerical simulations of incompressible isotropic turbulence. *Phys. Rev. Lett*, *3*(6), 064603.

Zimbardo, G., Greco, A., Sorriso-Valvo, L., Perri, S., Vörös, Z., Aburjania, G., ... Alexandrova, O. (2010). Magnetic turbulence in the geospace environment. *Space Sci. Rev.*, *156*(1-4), 89–134.

Table 1. Parameters for Simulations of Lagrangian Single-particle Diffusion and Two-particle Dispersion: magnitude of the static macroscopic magnetic field B_0, the root-mean-square of magnetic fluctuations B_{RMS} averaged over the full simulation time, Kolmogorov time scale τ_η, the large-eddy length scale $\mathsf{L_E}$, and the Kolmogorov microscale η_{kol}. Each simulation is performed on a grid of $N^3 = 1024^3$, and uses 8.3 million Lagrangian tracer particles in a homogeneous random distribution.

	B_0	B_{RMS}	$\tau_\eta(10^{-2})$	$\mathsf{L_E}$	η_{kol} (10^{-3})	Re	elongation
HNOVIS	–	–	4.47	3.56	3.46	7571	1
ANOVIS0	0.	1.10	5.15	2.81	3.59	7230	1
ANOVIS3	3.	1.09	5.74	5.56	3.79	7570	2

Table 2. Parameters for Simulations of Lagrangian Many-particle Dispersion: magnitude of the static macroscopic magnetic field B_0, the root-mean-square of magnetic fluctuations B_{RMS} averaged over the full simulation time, Kolmogorov time scale τ_η, the large-eddy length scale $\mathsf{L_E}$, and the Kolmogorov microscale η_{kol}. Each simulation is performed on a grid of $N^3 = 1024^3$ and uses 4.5 million particles initialized into droplets.

	B_0	B_{RMS}	$\tau_\eta(10^{-2})$	$\mathsf{L_E}$	η_{kol} (10^{-3})	Re	elongation
HPUFF	–	–	4.20	3.70	3.55	10570	1
APUFF0	0.	1.78	4.89	2.49	3.83	5640	1
APUFF3	3.	1.17	4.82	2.57	3.80	5940	2